

Chapter 6

The practical implementation of spectral leakage theory in global surface wave tomography

Abstract.

We investigate the effect of uneven ray path coverage in global surface wave tomography. An inhomogeneous distribution of seismicity may bias tomographic models because certain areas are better sampled than others. It is possible to suppress the bias due to the inhomogeneous ray path coverage by using a linear inversion technique known as spectral leakage theory that differs only from the general least squares solution in the way that data are weighted. In spectral leakage theory, the data weighting matrix is the summation of the data covariance matrix and a matrix that accounts for the simulation of even ray path coverage. Spectral leakage theory is applied together with surface wave scattering theory in an inversion of phase velocity measurements for Love waves between 40 s and 150 s. Surface wave scattering theory has a larger validity in media with small-scale heterogeneity for which the conditions for the ray theoretical great circle approximation are not satisfied. Phase velocity maps for Love waves at 40 s and 150 s from the undamped spectral leakage inversion are compared with those from the least squares inversion without any regularisation condition in use. It is concluded from the comparison of surface wave models from these two linear inversions that the simulation of homogeneous ray path coverage in the global surface wave tomographic experiment improves the phase velocity maps that correlate better with tectonic features.

6.1 Introduction

High-resolution tomographic surface wave models of the Earth may contain significant errors because of the limitations of the methodology in surface wave tomography; First,

most surface wave tomographic experiments are based on the ray theoretical great circle theorem (Jordan, 1978; Trampert and Woodhouse, 1995; van der Lee and Nolet, 1997; Curtis *et al.*, 1998) which is only valid in smooth media. However, present-day surface wave models show characteristic length-scales of heterogeneity that are at the limits to justify the use of the great circle approximation in global and regional, high-resolution surface wave models (Passier and Snieder, 1995; Spetzler *et al.*, 2001). It is therefore important to take the scattering of surface waves into account in order to obtain surface wave Earth models with a higher resolution than is currently possible. Second, due to the practical limitations of inversion techniques in surface wave tomography, it is common to truncate the series of basis functions that is used to model the structure of the Earth to a certain (arbitrary) level. The truncation of the expansion of basis functions may lead to spectral leakage which means that the contribution of small-scale structures of heterogeneity that is not accounted for in the inversion may leak into the inverted tomographic model of inhomogeneity (Trampert and Snieder, 1996). The spectral leakage problem is related to the uneven ray path coverage in surface wave tomography on the globe (Gudmundsson *et al.*, 1990; Snieder *et al.*, 1991; Iyer and Hirahara, 1993). This in its turn is due to the nature of global tomographic wave experiments where earthquakes are used as the source of waves to probe the interior of the Earth.

The main focus in this article is on the spectral leakage problem in a global surface wave tomographic experiment using phase velocity measurements for Love waves between 40 s and 150 s. The surface wave data are from Trampert and Woodhouse (2001). Instead of making use of the great circle approximation, we benefit from the methodological improvements in surface wave scattering theory of Spetzler *et al.* (2001). The employed scattering theory of surface waves is a linear theory where the relative phaseshift is expressed as a volume integration of the relative velocity perturbation field multiplied by the Fréchet kernel. The reader is referred to Spetzler *et al.* (2001) for more information about surface wave scattering theory.

In order to compensate for the uneven distribution of earthquake and receiver positions in global surface wave tomography, we make use of the work of Trampert and Snieder (1996) who develop a least-squares technique to suppress the artifacts due to spectral leakage. The difference between the least squares solution taking account of the spectral leakage problem and the general least squares inversion (Tarantola, 1987; Menke, 1989) is the way that data are weighted. In Trampert and Snieder (1996), the data weighting matrix is the sum of the data covariance matrix and another matrix that is used to suppress the effects of spectral leakage.

The elements of the matrix that accounts for the effects of spectral leakage in the spectral leakage inversion is only defined for scattering theory and not for ray theory. This is because these matrix elements correspond to the volume integration over the sphere of the Fréchet kernels due to the source-receiver configurations under consideration. For ray theory, the Fréchet kernel is the delta-function, and the integration of two delta-functions is not defined mathematically.

The spectral leakage problem is considered by others in geophysics. For instance, Dziewonski and Anderson (1981) eliminate the bias introduced by unequally distributed seismicity in lateral structures by taking the average of body wave traveltimes for

Earth sections with equal area in order to obtain the one dimensional PREM model. Snieder *et al.* (1991) set up a synthetic experiment using an artificial set of evenly distributed source-receiver pairs and a realistic set of inhomogeneous ray path coverage. In this way, they show that the spectral leakage problem originates from unevenly distributed source-receiver pairs. The spectral leakage problem is not only applicable to a truncation of the series of basis functions as it is the case in surface wave tomography (Trampert and Woodhouse, 1995; Trampert and Woodhouse, 2001; Spetzler *et al.* 2001). Arkani-Hamed *et al.* (1994) who work with the Earth's magnetic field, expand the perturbation field of a magnetic anomaly map into spherical harmonics with angular degrees from 15 to 60. In that case, the effect of spectral leakage may be relevant for the lower and upper truncation of the series of the spherical harmonics.

In section 6.2, the theory correcting for the spectral leakage problem as found in Trampert and Snieder (1996) is briefly reviewed. It is explained in section 6.3, how the least squares solution from spectral leakage theory is combined with surface wave scattering theory in global surface wave tomography. The surface wave tomographic models obtained in the spectral leakage inversion of phase velocity measurements for Love waves at 40 s and 150 s are discussed in section 6.4, while a discussion and conclusions are given in section 6.5.

6.2 Theory

In this section, we explain the basic principles behind spectral leakage theory which is described in detail by Trampert and Snieder (1996) and Snieder and Trampert (1999). In general, the model parameter $m(x)$ at point x containing the complete set of basis functions $B_j(x)$ with the coefficients m_j can be decomposed into the part $m_L(x)$ which is the basis function expansion until the (arbitrary) truncation level L , and the part $m_\infty(x)$ that is the infinite series of the remaining basis functions, thus

$$m(x) = \sum_{j=1}^{\infty} m_j B_j(x) = m_L(x) + m_\infty(x), \quad (6.1)$$

with

$$m_L(x) = \sum_{j=1}^L m_j B_j(x), \quad \text{and} \quad m_\infty(x) = \sum_{j=L+1}^{\infty} m_j B_j(x). \quad (6.2)$$

Following the notation of Menke (1989), the datum d_i in continuous inverse theory is given by

$$d_i = \int G_i(x) m(x) dx + e_i, \quad (6.3)$$

where $G_i(x)$ is the continuous data kernel and e_i is the error of datum d_i . By inserting the series of basis functions in Eq. (6.1) for the model parameter $m(x)$ in the datum in Eq.

(6.3), the data can be related to the infinitely dimensional discrete model vector with the coefficients m_j . Hence,

$$d_i = \sum_{j=1}^{\infty} A_{ij} m_j + e_i, \quad (6.4)$$

where the modeling matrix elements

$$A_{ij} = \int G_i(x) B_j(x) dx, \quad (6.5)$$

are the projection of the data kernel $G_i(x)$ on the basis functions $B_j(x)$ (Snieder and Trampert, 1999). In more general terms, the discrete forward problem in eq. (6.4) is written as

$$\mathbf{d} = \mathbf{A}\mathbf{m} + \mathbf{e}, \quad (6.6)$$

which is the well-known linear forward problem in vector form (Tarantola, 1987; Menke, 1989). Given the truncation level L , the least squares solution to the linear problem in Eq. (6.6) is given by

$$\tilde{\mathbf{m}}_L = \mathbf{A}_L^{-g} \mathbf{d}, \quad (6.7)$$

with the inverse of the modeling matrix \mathbf{A}_L in the least squares sense given by

$$\mathbf{A}_L^{-g} = \left(\mathbf{A}_L^t \mathbf{C}_d^{-1} \mathbf{A}_L + \mathbf{C}_{m,L}^{-1} \right)^{-1} \mathbf{A}_L^t \mathbf{C}_d^{-1}. \quad (6.8)$$

The modeling matrix \mathbf{A}_L is constructed for the model parameters until the (arbitrary) truncation level L , and the covariance matrix for the truncated prior model vector \mathbf{m}_L and the observed data \mathbf{d} is denoted by $\mathbf{C}_{m,L}$ and \mathbf{C}_d , respectively. (Tarantola, 1987; Menke, 1989)

The observed data in the general linear problem in Eq. (6.6) are affected by both vectors \mathbf{m}_L and \mathbf{m}_∞ of the coefficients m_j , hence

$$\mathbf{d} = \mathbf{A}_L \mathbf{m}_L + \mathbf{A}_\infty \mathbf{m}_\infty + \mathbf{e}, \quad (6.9)$$

where \mathbf{A}_∞ is the modeling matrix for the infinitely-dimensional vector \mathbf{m}_∞ . The expression for the observed data in Eq. (6.9) is inserted in the least squares solution in Eq. (6.7), thereby enabling us to show the effect of spectral leakage. According to Snieder and Trampert (1999), the truncated vector $\tilde{\mathbf{m}}_L$ of the estimated model vector to the truncation level L is given by

$$\tilde{\mathbf{m}}_L = \mathbf{m}_L + \left(\mathbf{A}_L^{-g} \mathbf{A}_L - \mathbf{I} \right) \mathbf{m}_L + \mathbf{A}_L^{-g} \mathbf{A}_\infty \mathbf{m}_\infty + \mathbf{A}_L^{-g} \mathbf{e}. \quad (6.10)$$

The last three terms in Eq. (6.10) are responsible for the discrepancy in the estimated model from the true model \mathbf{m}_L . The second term and the last term account for the limitations in finite-resolution within the subspace for the vector \mathbf{m}_L of the model coefficients,

and the effects of the observational data errors \mathbf{e} . The remaining term $\mathbf{A}_L^{-g} \mathbf{A}_\infty \mathbf{m}_\infty$ is the projection of the data contribution from the vector \mathbf{m}_∞ of model coefficients onto the truncated vector $\tilde{\mathbf{m}}_L$ of model coefficients. This term describes spectral leakage.

The cure for spectral leakage is given in Trampert and Snieder (1996) and Snieder and Trampert (1999). In the least squares sense, they show how the solution for the truncated model vector including the spectral leakage correction is derived. In this paper, only the simplest case that the covariance matrix for the data $\mathbf{C}_d = \sigma_d^2 \mathbf{I}$, and for the model vectors $\mathbf{C}_{m,L} = \sigma_{m,L}^2 \mathbf{I}$ and $\mathbf{C}_{m,\infty} = \sigma_{m,\infty}^2 \mathbf{I}$, is considered. Trampert and Snieder (1996) define $\alpha^2 = \sigma_d^2 / \sigma_{m,L}^2$ and $\beta^2 = \sigma_d^2 / \sigma_{m,\infty}^2$. The least squares solution $\tilde{\mathbf{m}}_L^W$ with the spectral leakage correction is given by

$$\tilde{\mathbf{m}}_L^W = \left(\mathbf{A}_L^t \mathbf{W} \mathbf{A}_L + \left(\frac{\alpha^2}{\beta^2} \right) \mathbf{I} \right)^{-1} \mathbf{A}_L^t \mathbf{W} \mathbf{d}, \quad (6.11)$$

with the anti-leakage matrix

$$\mathbf{W} = \left(\mathbf{A}_\infty \mathbf{A}_\infty^t + \beta^2 \mathbf{I} \right)^{-1}. \quad (6.12)$$

The anti-leakage matrix in Eq. (6.12) is the inverse of the sum of the matrix $\mathbf{A}_\infty \mathbf{A}_\infty^t$ that is used to suppress the spectral leakage effect and the diagonal matrix $\beta^2 \mathbf{I}$ that includes the variance of the data and the infinitely dimensional model vector \mathbf{m}_∞ .

6.3 Spectral leakage theory in global surface wave tomography

In this section, it is explained how the inverse problem with the spectral leakage correction is set up in global surface wave tomography using phase velocity measurements. The relative phaseshift d_{scat} due to the scattering of surface waves is calculated as a summation of the spherical harmonics coefficients C_l^m multiplied by the Fréchet kernel $K_{l,m}^{scat}$ for angular degree l and order m using diffraction theory. Scattering theory for unconverted surface waves is derived in Spetzler *et al.* (2001). The relative phaseshift is given by

$$d_{scat} = \sum_{l=0}^{l_{max}} \sum_{m=-l}^l C_l^m K_{l,m}^{scat}, \quad (6.13)$$

with the maximum angular degree of the spherical harmonic expansion denoted by l_{max} , which is a finite number in practical applications. The Fréchet kernel $K_{l,m}^{scat}$ for angular degree l and order m is the integration of the sensitivity function $K^{scat}(R, \theta, \varphi)$ due to the scattering of surface waves and the spherical harmonic $Y_l^m(\theta, \varphi)$ over the sphere Ω . Hence,

$$K_{l,m}^{scat} = \int_{\Omega} K^{scat}(R, \theta, \varphi) Y_l^m(\theta, \varphi) d\theta d\varphi. \quad (6.14)$$

The reader is referred to Fig. 1 in Spetzler *et al.* (2001) for examples of the sensitivity function $K^{scat}(R, \theta, \varphi)$. By comparing the expression for the modeling matrix in Eq. (6.5) with the Fréchet kernel in eq. (6.14), we identify that the data kernel $G_i(x)$ corresponds to $K^{scat}(R, \theta, \varphi)$ and the basis functions $B_j(x)$ are the spherical harmonics $Y_l^m(\theta, \varphi)$. It is shown on p. 154 in Snieder and Trampert (1999) that the matrix product $\mathbf{A}_\infty \mathbf{A}_\infty^t$ in Eq. (6.12) using the notation for surface wave scattering theory can be written as

$$\{\mathbf{A}_\infty \mathbf{A}_\infty^t\}_{ij} = \int_{\Omega} K_i^{scat}(R, \theta, \varphi) K_j^{scat}(R, \theta, \varphi) d\theta d\varphi - \{\mathbf{A}_L \mathbf{A}_L^t\}_{ij}, \quad (6.15)$$

where the subindex in the sensitivity functions indicate the source-receiver pairs i and j . In terms of surface wave scattering theory, it makes sense to evaluate the integration of the two weighting functions in Eq. (6.15), because they are defined everywhere over the sphere. In contrast, the integration part (known as the Gram matrix, Trampert and Snieder, 1996) in Eq. (6.15) is not defined for ray theory; the data kernel $K_i^{ray}(R, \theta, \varphi)$ due to ray theory on the sphere is a delta-function depending on the spherical coordinates. The integration of the product of two delta-functions on the sphere yields zero, so the Gram matrix is not defined in terms of ray theory. In addition, the application of the ray-theoretical great circle approximation in global surface wave tomography is limited to structures with angular degrees of the spherical harmonics smaller than $l = 30$ for Love waves at 40 s and $l = 20$ for Love waves at 150 s (Spetzler *et al.*, 2001).

The anti-leakage matrix \mathbf{W} in Eq. (6.12) has the number of rows and columns equal to the number of data applied in the inverse problem. If many data are used in the tomographic experiment, the matrix \mathbf{W} is large which may cause problems when storing it in the computer memory (or even on the hard-disc). In the global surface wave tomographic experiment using phase velocity measurements, the elements of the matrix $\mathbf{A}_\infty \mathbf{A}_\infty^t$ in the anti-leakage matrix \mathbf{W} are calculated from the matrix product

$$\{\mathbf{A}_\infty \mathbf{A}_\infty^t\}_{ij} = \sum_{s=L+1}^{\infty} \{\mathbf{A}_\infty\}_{is} \{\mathbf{A}_\infty^t\}_{sj}, \quad (6.16)$$

instead of using the expression for $\mathbf{A}_\infty \mathbf{A}_\infty^t$ in Eq. (6.15) for which the evaluation of the integral is numerically demanding. In practice, the summation over s in eq. (6.16) is limited to a certain maximum angular degree l_{max} of the spherical harmonics expansion much higher than the truncation level L .

The off-diagonal elements of the anti-leakage matrix in Eq. (6.12) are significant if different source-receiver pairs are parallel and close to each other or if different source-receiver minor arcs or major arcs cross at an oblique angle so that their Fresnel zones overlap. In general, the anti-leakage matrix \mathbf{W} is symmetric, and it is found that \mathbf{W} is sparse as well for the Love wave dataset between 40 s and 150 s from Trampert and Woodhouse (2001). The sparseness of \mathbf{W} comes from the fact that many of the source-receiver pairs do not have overlapping Fresnel zones. However for Love waves at both 40 s and 150 s, several of the off-diagonal elements of the anti-leakage matrix are comparable with the diagonal elements of \mathbf{W} because the respective source-receiver pairs are close to each other. The matrix \mathbf{W} must therefore be inverted by brute force (such as Gaus-

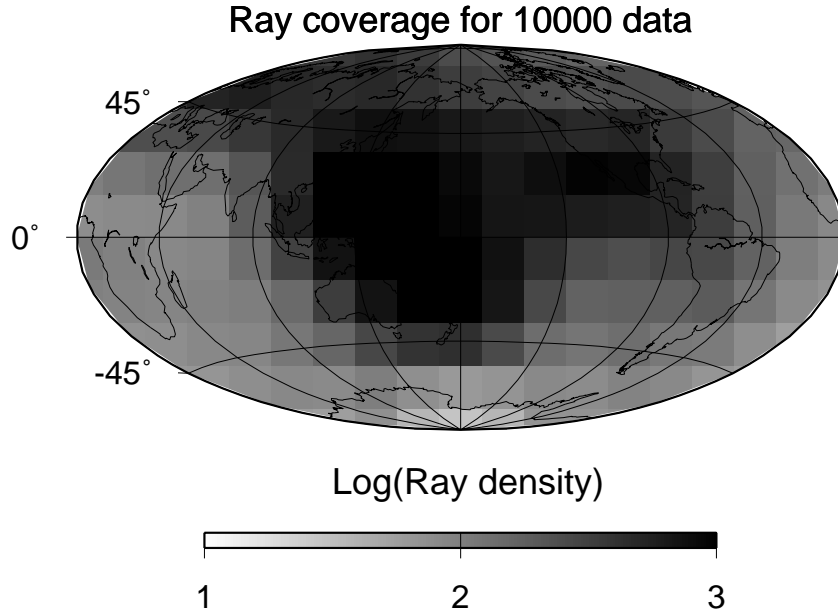


Figure 6.1: *The ray coverage density for the dataset of the 10000 relative phaseshifts for Love waves between 40 s and 150 s. The grey colour scale shows the logarithmic value of the ray path coverage density.*

Jordan elimination, see Press *et al.*, 1986) as the form of the sparse anti-leakage matrix is irregular.

In the inversion of phase velocity measurements for Love waves between 40 s and 150 s using spectral leakage theory, we apply 10000 surface wave data from Trampert and Woodhouse (2001). Note that all the global surface wave Earth models presented here are estimated from the same 10000 phase velocity measurements for Love waves between 40 s and 150 s. The ray density for the Love wave dataset of 10000 relative phaseshift measurements is shown in Fig. 6.1. Notice that the ray density is shown on a logarithmic-scale. It is clearly seen that the phase velocity models presented later in this paper are sampled with an uneven path distribution. We find the highest ray path coverage on the Pacific plate, in Eurasia and in North America while the poorest sampling rate is found on the Southern hemisphere with an emphasis on the Southpole.

The value of α in Eq. (6.11) is set to zero, which corresponds to an inversion without any damping. The value of β in Eq. (6.12) is chosen by trial and error using the conditions that the phase velocity maps from the spectral leakage inversion are stable. We found that the lowest value of β which is $\beta = 0.5$, satisfies this condition.

According to Eq. (6.10) the estimated model $\tilde{\mathbf{m}}_L$ differs from the true model \mathbf{m}_L because of the three distinct contributions that are $(\mathbf{R} - \mathbf{I})\mathbf{m}_L$ (resolution limitation), $\mathbf{A}_L^{-g}\mathbf{A}_\infty\mathbf{m}_\infty$ (spectral leakage effect) and $\mathbf{A}_L^{-g}\mathbf{e}$ (data error propagation). The resolution

matrix is given by $\mathbf{R} = \mathbf{A}_L^{-g} \mathbf{A}_L$ (Tarantola, 1987; Menke, 1989). Firstly, because there is no need for a regularisation condition in the spectral leakage inversion ($\alpha = 0$), the resolution matrix $\mathbf{R} = \mathbf{I}$ (see appendix A). Secondly, we use spectral leakage theory in the global phase velocity experiment, so the leakage term $\mathbf{A}_L^{-g} \mathbf{A}_\infty \mathbf{m}_\infty = \mathbf{0}$. The estimated surface wave models using spectral leakage theory are therefore only affected by the uncertainty from the data error propagation. Hence,

$$\tilde{\mathbf{m}}_L = \mathbf{m}_L + \mathbf{A}_L^{-g} \mathbf{e}. \quad (6.17)$$

The truncation level is $L = 20$ and $L = 10$ for Love waves at 40 s and 150 s, respectively, which assures stable surface wave models when applying spectral leakage theory. It is shown in Fig. 5 of Trampert and Snieder (1996) that mostly the lower degree basis functions, $Y_{l,m}$, just above the truncation level bias the highest degree spherical harmonics below the truncation level. The maximum angular degree and order of the Fréchet kernels that is used to compute the elements of the anti-leakage matrix in Eq. (6.12) is set to $l_{max} = 40$, because it is unlikely that higher degree spherical harmonics larger than $l_{max} = 40$ leak into the spherical harmonics with angular degrees smaller than the truncation level at angular degree $L = 20$ and $L = 10$ for Love waves at 40 s and 150 s, respectively.

6.4 Phase velocity maps from the spectral leakage inversion of relative phaseshifts

The relative phase velocity maps for Love waves at 40 s and 150 s corrected for the spectral leakage effect are shown in Fig. 6.2A and 6.3A, respectively. The surface wave models from the spectral leakage inversion are compared with those for Love waves at 40 s (Fig. 6.2B) and 150 s (Fig. 6.3B) which are retrieved in a common least squares estimation (see Eq. (6.8)) without any regularisation in use ($\mathbf{C}_d^{-1} = \mathbf{I}$, and $\mathbf{C}_{m,L}^{-1} = \mathbf{0}$). The reader is referred to appendix A for a discussion about the fairness of the comparison of the phase velocity models from the undamped spectral leakage inversion and the common least squares inversion without applying a regularisation condition. The grey-scale colour for the relative phase velocity perturbations in Fig. 6.2 and 6.3 is between $\pm 5\%$ compared to the PREM-model for Love waves at the respective periods in order to show detailed structures of all the phase velocity models presented here. However, the relative phase velocity perturbations in the inversion of the relative phaseshifts for Love waves at 40 s are between -15% and 17% , and for Love waves at 150 s the minimum perturbation is -7% and the maximum phase velocity perturbation is 9% . The surface wave models for Love waves at 40 s may seem identical which is an artifact due to the applied grey-scale colours ranging between $\pm 5\%$ for the relative velocity perturbations that are between -15% and 17% .

The difference between the phase velocity maps obtained in the two separate inversions are plotted in Fig. 6.4A for Love waves at 40 s and in Fig. 6.4B for Love waves at 150 s. The abbreviation ‘usli’ stands for the undamped spectral leakage inversion, and ‘cls’ refers to the common least squares inversion without applying any regularisation

condition. Unfortunately, the difference in relative phase velocity between the surface wave models from the undamped spectral leakage inversion and the common undamped least squares inversion is not entirely due to the effect of spectral leakage. There might be some contribution of data error propagation in the differences of relative phase velocity in Fig. 6.4A and 6.4B, because the inverse of the modeling matrix \mathbf{A}_L^{-g} is not the same in the spectral leakage inversion and in the common least squares inversion. A scale analysis of the difference between the inverse of the modeling matrix \mathbf{A}_L^{-g} in the spectral leakage estimation and in the least squares inversion that is compared to the inverse of the modeling matrix in the spectral leakage inversion has been carried out. This scale analysis reveals that the difference between the inverse of the modeling matrix in the spectral leakage inversion and in the least squares inversion is not negligible. On the other hand, the global surface wave experiment is well-constrained because we use many data and because we do not need to apply any damping in the inversion of phase velocity measurements using spectral leakage theory or the least squares estimation (see appendix A for a discussion of the comparison of the relative phase velocity models from the two separate linear inversions). We therefore believe that the contribution of data error is not significant in the global surface wave experiment. It is seen in Fig. 6.4 that the effect of the anti-leakage matrix is significant as there are large differences in the small-scale structures of the surface wave models obtained in the two kind of inversions. The characteristic wavelength of the differences in the small-scale relative phase velocity structure is comparable to the truncation level of the series of the spherical harmonics. Thus for the inversion of Love waves at 40 s the length-scale of differences of relative phase velocity is about $l \approx 20$ (or corresponding to 2000 km), and for the experiment with Love waves at 150 s the difference in structure has a characteristic length of $l \approx 10$ (or corresponding to 4000 km). This observation shows that the effect of spectral leakage is most important at the truncation level, which is as well shown by in Fig. 5 of Trampert and Snieder (1996).

Qualitatively, the phase velocity maps for Love waves at 40 s and 150 s from the undamped spectral leakage inversion correlate better with tectonic features than those from the common least squares inversion without applying a regularisation condition. For instant look at Fig. 6.5 where two sections of the Love wave model at 40 s from the two separate inversions are presented. The section for Fig. 6.5A and 6.5B contains the area with Africa, Tibet and the Carlsberg ridge, while the section for Fig. 6.5C and 6.5D is the region with South America, the East Pacific rise and the Chile rise. These two sections are the most clear examples for the Love wave models at 40 s. It is clearly seen from Fig. 6.3 that the phase velocity maps for Love wave at 150 s using the undamped spectral leakage solution have a better correlation with tectonic boundaries than the surface wave models obtained in the common least squares estimation without any regularisation condition in use. For examples in Fig. 6.3, we stress out the Carlsberg ridge, the South-West Indian ridge, the Hunter ridge and the Chile rise.

In Fig. 6.6, the unexplained variance that is a measure of how well the Love wave phase velocity maps explain the observed data, is plotted for values of $(\alpha/\beta)^2$ ranging from zero to 30. In general, the unexplained variance increases for increasing values of $(\alpha/\beta)^2$. Nevertheless, it is shown most clearly in the spectral leakage inversion for Love waves at 150 s that the value of α giving the minimum unexplained variance is not for

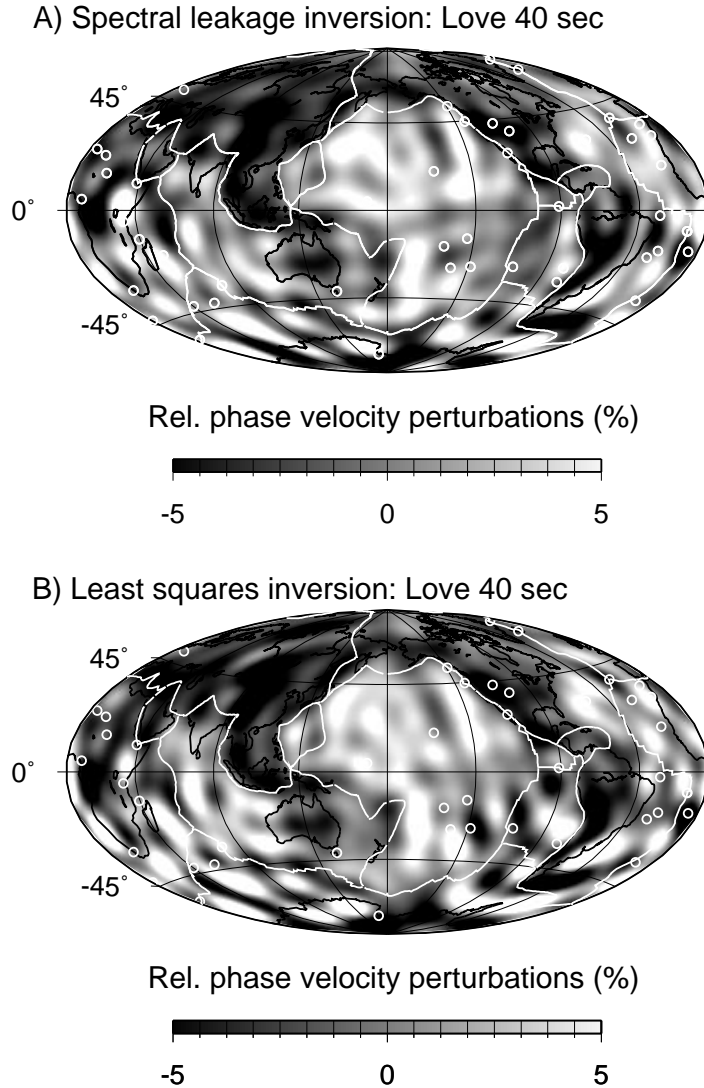


Figure 6.2: Global phase velocity Earth models for Love waves at 40 s. The white circles are hotspots, the white lines show the boundaries between tectonic plates and coastlines are drawn with the thick black lines. The variations in the relative phase velocity perturbations are given in percent on a scale $\pm 5\%$ with respect to the constant PREM model for Love waves at 40 s. The series of the spherical harmonics is truncated at the angular degree $L = 20$. A) The phase velocity map that is obtained in the inversion accounting for the spectral leakage problem. The parameters $\alpha = 0$ and $\beta = 0.5$. B) The phase velocity map that comes from the common least squares inversion without using any damping.

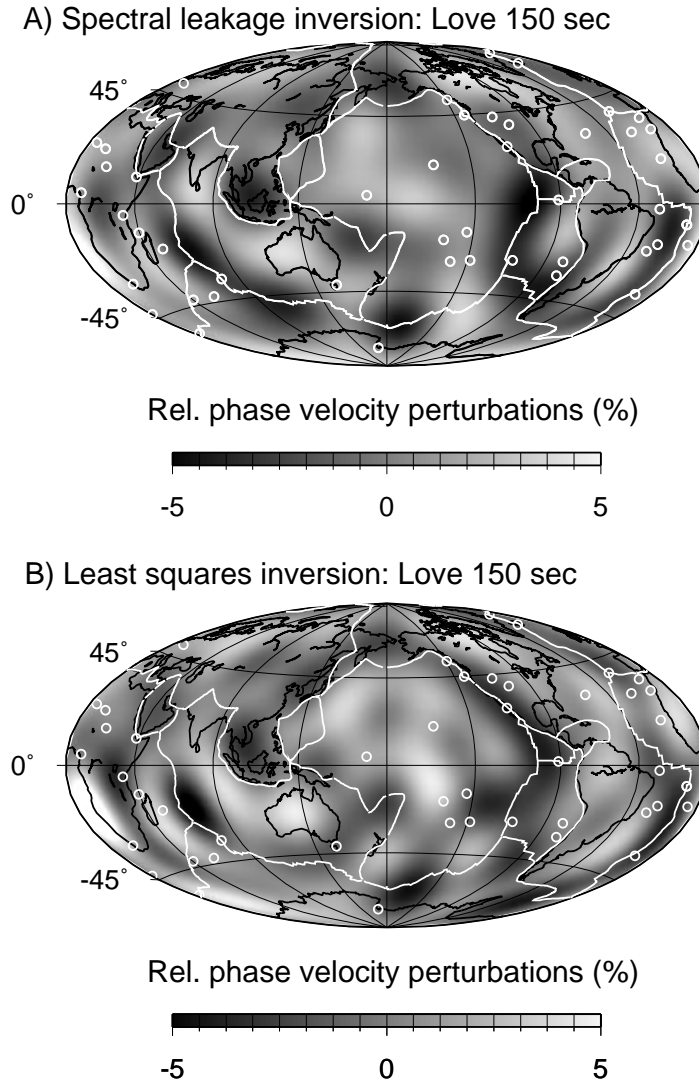


Figure 6.3: As in Fig. 6.2, but for this figure Love waves at 150 s are used in the two separate linear inversions without applying any damping. The series of the spherical harmonics is truncated at the angular degree $L = 10$. The variations in the relative phase velocity perturbations are given in percent on a scale $\pm 5\%$ with respect to the constant PREM model for Love waves at 150 s. A) The phase velocity map obtained in the inversion that suppresses the spectral leakage effect. The value of α is zero and β is set to 0.5. B) The phase velocity map that is retrieved from the common least squares inversion without using any regularisation condition.

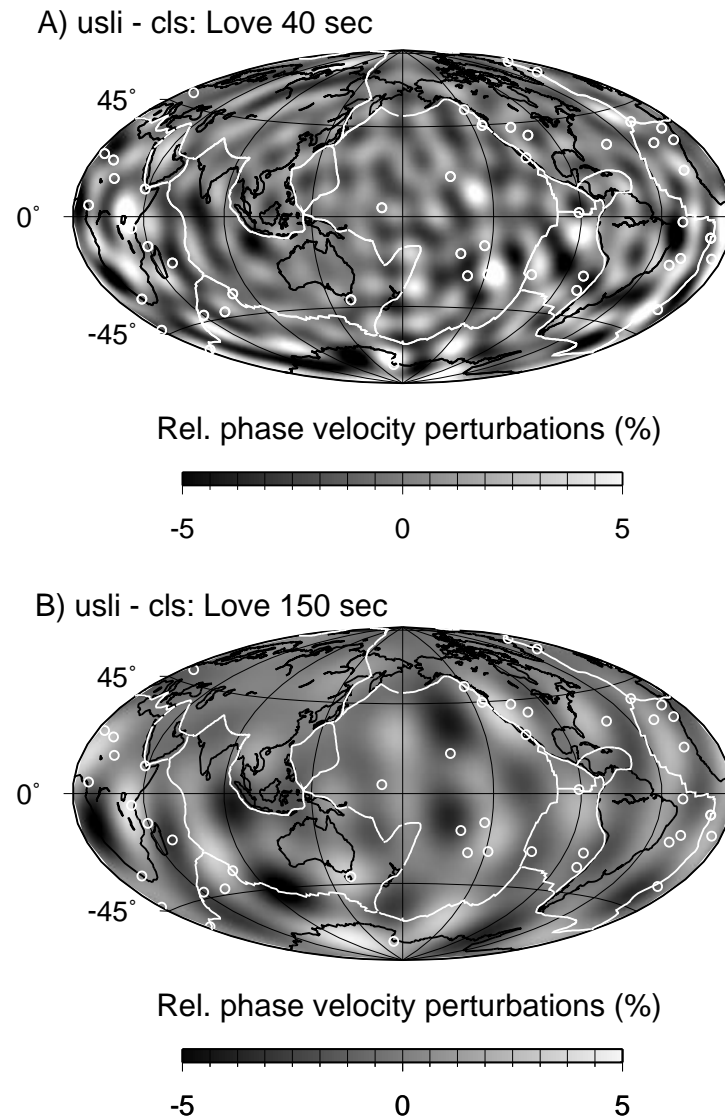


Figure 6.4: *The difference between the phase velocity maps obtained in the undamped spectral leakage inversion (usli) without any damping and the common least squares (cls) inversion with no regularisation condition in use. The convention for hotspots, plate boundaries and coast lines is the same as in Fig. 6.2. A) The inversion of relative phase-shifts for Love waves at 40 s. B) The inversion of the phase velocity measurements for Love waves at 150 s.*

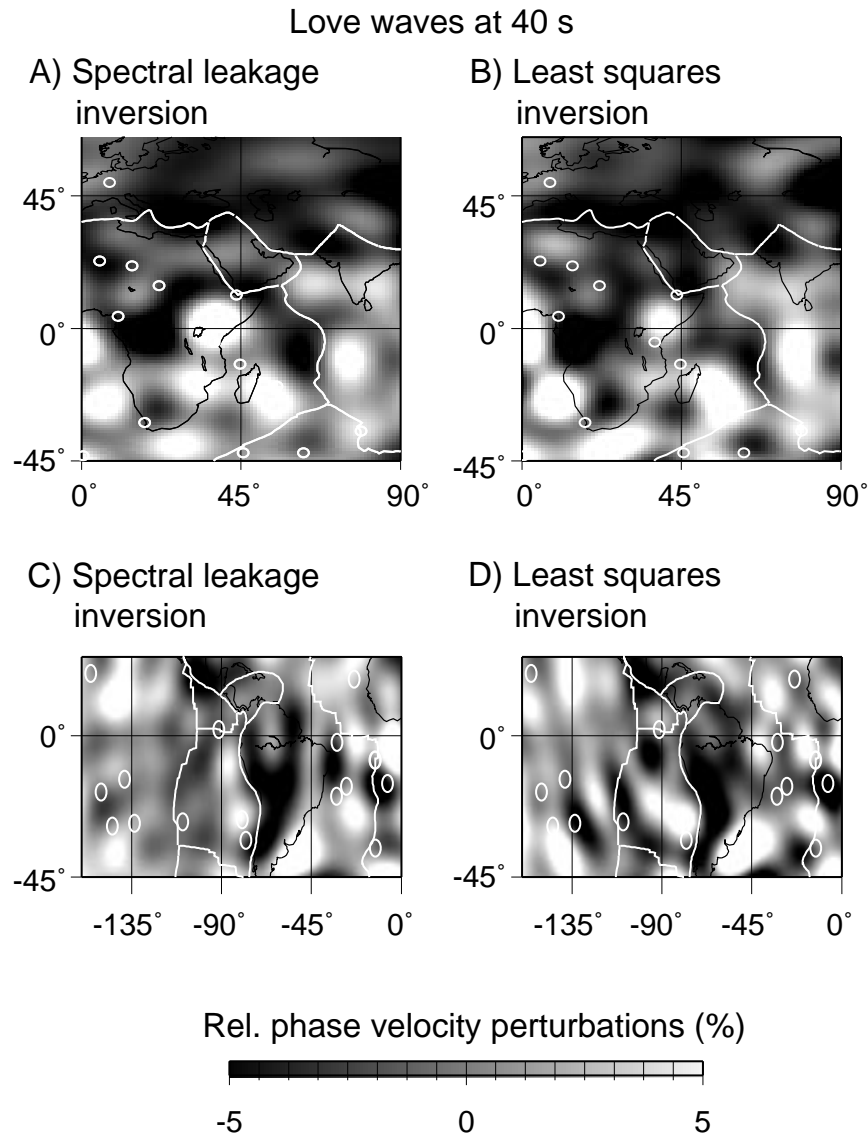


Figure 6.5: Selected sections of the phase velocity maps for Love wave at 40 s and 150 s that are shown in Fig. 6.2. The colour convention for hotspots, plate boundaries and coast lines is unchanged from Fig. 6.2. For A) and B), the section includes Africa, Tibet and the Carlsberg ridge. For C) and D), the section is the region with the east Pacific rise, the Chile rise and South America.

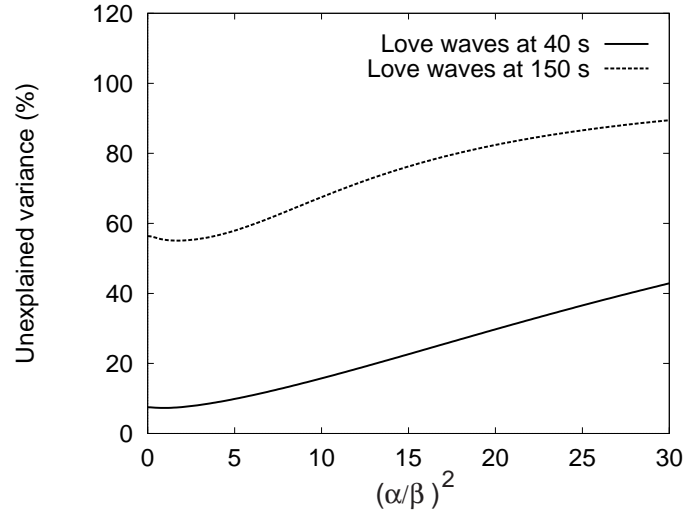


Figure 6.6: The unexplained variance in percent for different values of $(\alpha/\beta)^2$ in the spectral leakage inversion of phase velocity measurements for Love waves at 40 s and 150 s, respectively. If $(\alpha/\beta)^2$ is equal to zero, this corresponds to an inversion with no regularisation. The estimated phase velocity maps for Love waves at 40 s and 150 s converge towards the homogeneous PREM reference model as the value of $(\alpha/\beta)^2$ increases.

$\alpha = 0$ but for $\alpha \approx 2$. When $(\alpha/\beta)^2$ is large in the spectral leakage inversion, the estimated phase velocity models for Love waves at 40 s and 150 s are close to the homogeneous PREM reference model because a large value of $(\alpha/\beta)^2$ corresponds to an inversion with a restrictive regularisation condition.

6.5 Discussion and conclusions

The presented Love wave phase velocity models from the spectral leakage inversion are obtained without using any damping ($\alpha = 0$). This means that only the effects of data error propagation contribute to the surface wave models for Love waves at 40 s and 150 s which are estimated in the inversion of phase velocity measurements using spectral leakage theory.

The phase velocity maps for Love waves at 40 s and 150 s obtained in the spectral leakage inversion without any damping are compared with those that are estimated in a common least squares inversion without using any regularisation condition. Among these two linear inversion approaches, the surface wave models from the spectral leakage inversion correlate better with many tectonic features such as ridges (e.g. the Carlsberg ridge, the South-West Indian ridge, the Hunter ridge and the southern part of the Mid-Atlantic ridge) and rises (i.e. the East Pacific rise and the Chile rise).

Spectral leakage theory is numerically rather demanding, because the anti-leakage matrix must be inverted by brute force. Every time the number of data doubles it takes 8 times more processor time to invert the anti-leakage matrix (Press *et al.*, 1986). This problem imposes a limitation on the number of surface wave data that is feasible to invert for in a reasonable amount of time. For instance, the spectral leakage inversion of 10000 Love wave relative phaseshifts takes 2 day on a 250 MHz ultra-sparc machine, so an inversion of 20000 surface wave data takes 16 days. It would therefore be rewarding to find a way to invert the anti-leakage matrix much faster by exploiting the symmetric and sparse property of the anti-leakage matrix.

References

- Arkani-Hamed J., Langel R. A. and Purucker M. (1994). Scalar magnetic anomaly maps of the Earth from POGO and Magsat data, *J. Geophys. Res.* **99**, 24075-24090.
- Curtis A., Trampert J., Snieder R. and Dost B. (1998). Eurasian fundamental mode surface wave phase velocities and their relationship with tectonic structures, *J. Geophys. Res.* **103**, 26919-26947.
- Dziewonski M. A. and Anderson D. L. (1981) Preliminary reference Earth model, *Phys. Earth Planet. Inter.* **25**, 297-356.
- Gudmondsson O., Davies J. H. and Clayton R. W. (1990). Stochastic analysis of global traveltimes data: mantle heterogeneity and random errors in the ISC data, *J. Geophys. Res.* **102**, 25-43.
- Iyer H. M. and Hirahara K. (1993). *Seismic tomography; theory and practice* (Chapman and Hall.).
- Jordan T. H. (1978). A procedure for estimating lateral variations from low frequency eigenspectra data, *Geophys. J. R. astr. Soc.* **52**, 441-455.
- van der Lee S. and Nolet G. (1997). Upper mantle S-velocity structure of North America, *J. Geophys. Res.* **102**, 22815-22838.
- Menke W. (1989). *Geophysical data analysis: discrete inverse theory* (Academic Press, Inc.).
- Passier M. L. and Snieder R. (1995). Using differential waveform data to retrieve local S-velocity structure or path-averaged S-velocity gradients, *J. Geophys. Res.* **100**, 24061-24078.
- Press W. H., Flannary B. P., Teukolsky S. A. and Vetterling W. I. (1986). *Numerical recipes: the art of scientific computation* (Cambridge University Press, UK).

- Scales J. and Snieder R. (2000). The anatomy of inverse problems, *Geophysics* **65**, 1708-1710.
- Snieder R., Beckers J. and Neele F. (1991). The effect of small-scale structure on normal mode frequencies and global inversions, *J. Geophys. Res.* **96**, 501-515.
- Snieder R. and Trampert J. (1999). *Inverse problems in geophysics in wavefield inversion*, Ed. A. Wirgin (Springer Verlag, New York.).
- Spetzler J., Trampert J. and Snieder R. (2001). The effect of scattering in surface wave tomography, *Geophys. J. Int.* (Submitted).
- Tarantola A. (1987). *Inverse problem theory: methods for data fitting and model parameter estimation* (Elsevier, New York).
- Trampert J. and Woodhouse J. H. (1995). Global phase velocity maps of Love and Rayleigh waves between 40 and 150 seconds, *Geophys. J. Int.* **122**, 675-690.
- Trampert J. and Snieder R. (1996). Model estimations biased by truncated expansions: possible artifacts in seismic tomography, *Science* **271**, 1257-1260.
- Trampert J. and Woodhouse J. H. (2001). Assessment of global phase velocity models, *Geophys. J. Int.* (144), 165-174.

6.6 Appendix A: The comparison of the phase velocity maps from the undamped spectral leakage inversion and the common undamped least squares inversion

According to Eq. (6.8), the inverse of the modeling matrix \mathbf{A}_L in the least squares solution using $\mathbf{C}_d^{-1} = \mathbf{I}$ and $\mathbf{C}_{m,L}^{-1} = \mathbf{0}$ is given by

$$\mathbf{A}_L^{-g} = \left(\mathbf{A}_L^t \mathbf{A}_L \right)^{-1} \mathbf{A}_L^t. \quad (6.18)$$

By using spectral leakage theory in Eq. (6.11), the inverse of the modeling matrix for $\alpha = 0$ (no damping) is simplified to

$$\mathbf{A}_L^{-g} = \left(\mathbf{A}_L^t \mathbf{W} \mathbf{A}_L \right)^{-1} \mathbf{A}_L^t \mathbf{W}. \quad (6.19)$$

The only difference between the inverted modeling matrix \mathbf{A}_L^{-g} in eq. (6.18) and Eq. (6.19) is the anti-leakage matrix \mathbf{W} , which is applied to suppress the effects of spectral leakage.

Next according to Tarantola (1987) and Menke (1989), the model resolution matrix \mathbf{R} is given by

$$\mathbf{R} = \mathbf{A}_L^{-g} \mathbf{A}_L. \quad (6.20)$$

The inverse of the modeling matrix from the common least squares solution without using any regularisation condition in Eq. (6.18) and from the undamped spectral leakage estimation in Eq. (6.19) are inserted in the expression for the model resolution matrix in Eq. (6.20). Hence for the common least squares inversion without any regularisation condition in use, we get that

$$\mathbf{R} = \left(\mathbf{A}_L^t \mathbf{A}_L \right)^{-1} \mathbf{A}_L^t \mathbf{A}_L = \mathbf{I}, \quad (6.21)$$

and for the undamped spectral leakage inversion, the model resolution matrix is

$$\mathbf{R} = \left(\mathbf{A}_L^t \mathbf{W} \mathbf{A}_L \right)^{-1} \mathbf{A}_L^t \mathbf{W} \mathbf{A}_L = \mathbf{I}, \quad (6.22)$$

which is always the case for a well-conditioned overdetermined inverse problem (p. 67 in Menke, 1989).

In order to verify if the global surface wave experiment for Love waves at 40 s and 150 s is a well-posed inverse problem, the trace of the model resolution matrix is calculated in the spectral leakage inversion without any damping and the common least squares solution without any regularisation condition in use. For both separate inversions, we find that the trace of the resolution matrix for the model parameters is equal to the number of model parameters used in the inversions. The positive result of the calculation of the trace of the model resolution matrix indicates that the model resolution matrices in the two kind of undamped inversions have no zero-eigenvalues. The global surface wave experiment for Love waves between 40 s and 150 s is therefore well-conditioned either using spectral leakage theory with $\alpha = 0$ or using the common least squares estimation without any regularisation condition. The comparison of the phase velocity maps from the two separate inversions is therefore considered to be fair.

